

Article

# Comparative Analysis and Design of the Shielding Techniques in WPT Systems for Charging EVs

Linlin Tan <sup>1</sup>, Kamal Eldin Idris Elnail <sup>1,\*</sup>, Minghao Ju <sup>2</sup> and Xueliang Huang <sup>1</sup>

<sup>1</sup> School of Electrical Engineering, Southeast University, No. 2 Sipailou, Nanjing 210096, China; tanlinlin@seu.edu.cn (L.T.); xlhuang@seu.edu.cn (X.H.)

<sup>2</sup> Shanghai Aerospace Control Technology Institute, No. 1555, Zhongchun Road, Minhang District, Shanghai 201109, China; mighaoju803@163.com

\* Correspondence: elneelka@hotmail.com; Tel.: +86-25-8379-2260

Received: 16 April 2019; Accepted: 25 May 2019; Published: 2 June 2016



**Abstract:** Wireless power transfer (WPT) systems for charging Electric Vehicles (EVs) have gained extensive attention due to their many advantages. However, human exposure to electromagnetic fields (EMFs) has become a serious concern in high-power cases. In this paper, shielding techniques, including magnetic, metallic, and resonant reactive current shields, are investigated. Finite element method software is used to evaluate and compare the shielding effectiveness, charger weight, and system performance. The results show that the resonant reactive current shielding has a low EMF level with reasonable system efficiency and acceptable charger weight. In addition, 5 kW with 15 cm air gap WPT chargers were built to validate the simulation results.

**Keywords:** shielding techniques; resonant reactive current shield; EMF; shielding effectiveness

## 1. Introduction

Recently, the increased demand for using green energy has necessitated the use of electric vehicles (EVs) to reduce the greenhouse gas (GHG) emissions [1]. Moreover, using EVs in the transportation sector will diversify the energy resources and reduce the dependence on petroleum products [2,3]. Since EV batteries need to be recharged regularly, there are two ways to recharge EVs batteries: conductive charging, which uses cables to transfer power from the charging station to the battery [2,4], and the counterpart is wireless power transfer (WPT) chargers which transfer the power using an alternating magnetic field through the air gap between two inductively coupled coils [5–7].

Inductively coupled links in WPT systems are considered loosely coupled transformers. Therefore, a huge amount of the magnetic flux generated by the primary coil is leaked around the charger [8]. Consequently, the increasing use of the WPT charging systems for EVs and for the other applications will increase the electromagnetic emissions. Therefore, the EMF biomedical effects on the human bodies and interference with concerning electronic devices must be seriously considered. To overcome these problems, several magnetic shielding techniques have been widely used to mitigate the EMF leakage, and to ensure that the WPT system is complying with the standards regarding the electromagnetic field (EMF) leaking out from the WPT systems.

Nowadays, many guidelines and standards have been developed to address the EMF limitation levels for EMF exposure to human bodies, and electromagnetic interference with electronic devices close by [9–11]. Shielding can be well-defined as the process of reducing the EMF in space by blocking the field using metal, magnetic materials, or any other shielding techniques. Therefore, the propagation of an electromagnetic wave from one region to another can be effectively controlled. Generally, the shielding techniques can be categorized into three types:

### 1.1. Passive Shielding

Passive shielding techniques include the use of conductive and ferromagnetic materials for suppressing or blocking the EMF. Firstly, using materials with low conductivity and high permeability such as ferrite can guide the magnetic flux through the desired path by providing an alternating path for magnetic flux [12]. Consequently, the leakage magnetic flux is significantly reduced, using a ferrite shielding method and electromagnetic field distribution as shown in Figure 1. Secondly, using conductive materials such as aluminum (Al), circulating eddy currents will be induced in these materials when exposed to alternating magnetic fields. These currents will generate magnetic fields in the opposite direction of the source and therefore a part of the incident magnetic field will be cancelled out as depicted in Figure 2 [13].

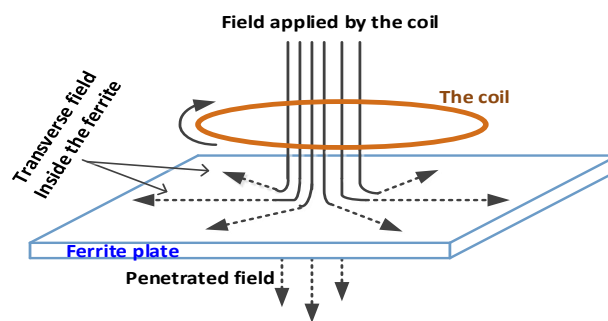


Figure 1. Passive shielding using ferrite [14].

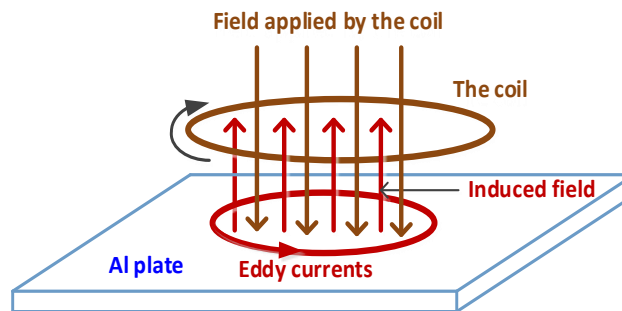


Figure 2. Passive shielding using conductive materials [14].

A serious problem in WPT systems for the EVs charging is that the Tx and Rx coils are physically separated, which imposes a large air gap. Thereby, when using conductive shielding, it is impossible for the conductive plates to cover that large air gap, particularly in EVs charging systems, which leads to significant leakage of the magnetic field. Authors in [15] investigated the influence of Al plates on the WPT system and the results show that the resonant frequency is changed due to the environmental change, and the transmission efficiency is decreased. The EMF shielding in WPT system generally adopts the method of metal shielding because it is simple and considered an appropriate shielding method for the low-power low-frequency WPT systems. Due to the field reflection and power losses, the conductive shield can not always be the suitable to use in a WPT system, especially in high power systems [16].

Three case studies are proposed to evaluate the WPT system's performance and EMF level in [17] including: WPT coils only, WPT coils with ferrite, and WPT coils with both ferrite core and Al plate. The ANSYS Maxwell Finite Element Method (FEM) solver is used for simulation and comparison. The results show that the magnetic flux density directly above and below the shield is significantly reduced due to the guided flux by the ferrite and suppressing effects by the Al plates in case 3 compared to the two other cases. Coils with ferrite core has a higher power transfer efficiency (91%), while adding Al palates reduced the system performance to 86.9%. Moreover, the coils without

ferrite core and Al plates have lower power transfer efficiency (79.6%). Therefore, in the practical WPT systems, the metallic shielding is composed of ferromagnetic material and conductive material together to reduce the magnetic field and enhance the magnetic coupling. However, the core and shielding structure and dimensions should carefully be designed [18]. In [19], magnetic field mitigation techniques for the WPT system are investigated. Three types of different material sheets are used as shielding including: aluminum, copper, and ferrite with different thickness. The system is tested for low power transfer and low frequency (30 W @ 20 kHz). The results show that the high conductivity of the metal panels of copper and aluminum produced relevant eddy current losses leading to reduction of the system efficiency dramatically. Using the high permeability and low losses materials leads to improving the system performance. Therefore, the ferrite shielding system has high efficiency and shielding effectiveness compared to the two other shielding materials.

Metal brushes are used in [20] to connect the vehicle bottom plate to the vertical ground plate to improve the passive shielding effectiveness. However, that will limit the EVs mobility as well as the resulting risk coming from the exposed conductive plate on the road. The passive shielding method is simple to apply; however, it has a relatively high cost, fails in high power applications, and increases the pad weight. Moreover, conductive materials significantly reduce the mutual inductance between two coils [14].

### 1.2. Active Shielding

In the active shielding technique, another power source is used to power the shielding coil as presented in Figure 3 or using the WPT coil current and inverting the winding to generate a counter EMF. To produce a robust EMF cancellation the amplitude and the phase of the current in the shielding coils must be carefully calculated [21,22]. A new active shielding method for I-type WPT system from the Korea Advanced Institute of Science and Technology (KAIST) is introduced in [21]. The cancel coil is added to the pick-up pad only, and the optimum space between the canceling coil and the main coil and the optimum number of turns of the canceling coil are determined. Moreover, adding core to the canceling coil is investigated, the results show that extending the core will enhance the cancellation effectiveness. Evidently, this method will increase the system complexity and cost. Moreover, it will decrease the general system performance [23].

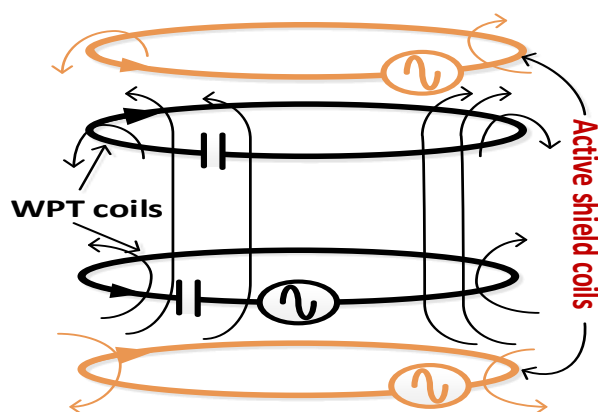


Figure 3. Active shielding using additional power sources.

### 1.3. Resonant Reactive Current (RRC) Shielding

A resonant reactive current shielding technique depends on the Lenz's law; when the magnetic field produced by the WPT coils couples with the shield coils, a current will be induced in these coils as presented in Figure 4. Therefore, this current will generate a canceling magnetic field. In [24], the resonant reactive shield is designed using two coils, one for phase detection, and the other for shielding. The modified phase shift method leads to generating a 180-degree phase different canceling magnetic field. However, the position of these two coils is the significant challenge for this design

especially in EV charging applications. Double-shield coils with four-capacitors as phase shifter resonant reactive shield design is proposed in [25]. The design can generate a sufficient canceling magnetic field. However, in this design, the two shielding coils must be positioned vertically between the WPT coils which are not suitable for EV chargers.

Appropriately adjusting the shield loop impedance will produce the appropriated canceling magnetic field [25,26]. Moreover, the shielding coils position has a significant effect on the shielding effectiveness [27,28]. It is clear that the resonant reactive current shielding method is simple, cheap, and suitable for high power applications; moreover, it can reduce the pad weight [29].

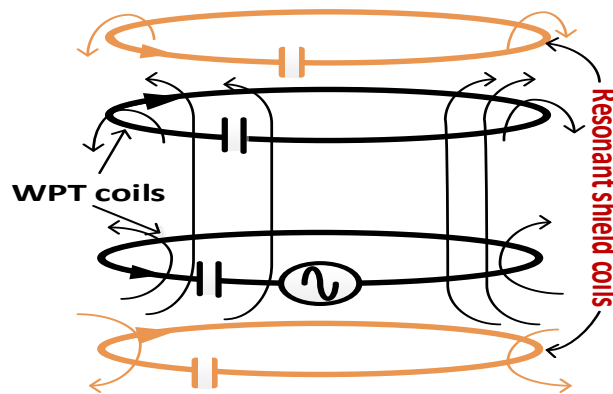


Figure 4. Resonant reactive current shielding.

The operative shielding method is the combination between the ferromagnetic materials as a passive shielding and resonant reactive current loops shielding for high frequencies high power systems, or with the conductive shielding for low frequencies' light power systems.

From the introduced previous works, there are many studies that have considered the shielding techniques and compared between them. However, most works carry out the comparison between the magnetic and conductive shielding compared to the system without shielding. Therefore, it is necessary to compare these two types of shielding to the resonant reactive current shielding method.

In this paper, shielding techniques including magnetic shielding, conductive shielding, and resonant reactive current shielding are discussed and compared. In addition, the electromagnetic environment surrounding the designed chargers is assessed and compared using FEM software ANSYS Maxwell (16) and by the measurement for the proposed shielding techniques. Power transferred and system efficiency are considered for each shielding type. The EMF environment surrounding the three chargers is extensively evaluated and compared. Circular coils and circular ferrite cores and aluminum sheets are used to design 5 kW, 85 kHz, 15 cm air gap for simulation and physical prototype. The results show that the resonant reactive shielding technique has the highest shielding effectiveness with acceptable system performance and good pad weight.

## 2. Shielding Effectiveness (SE)

Shielding effectiveness (SE) is a parameter used for shielding evaluation, which is defined as the ratio between the incident magnetic field intensity ( $H_i$ ) and the magnetic field intensity transmitted through the shield ( $H_t$ ) at a given distance from the magnetic source [30]:

$$SE = 20 \log_{10} \left| \frac{\vec{H}_i}{\vec{H}_t} \right|. \quad (1)$$

There are three methods used by the EMC community to approximate the shielding effectiveness of the materials including Maxwell's laws and equations, Schelkunoff's approximation method,

and Kirchhoff's approximation method [31]. Schelkunoff's approximation is made based on the transmission line model as illustrated in Figure 5.  $SE(dB)$  formula is given [32]:

$$SE = SE_A + SE_R + SE_M. \quad (2)$$

$SE_A$  is the absorption loss of the shielding material,  $SE_R$  is the single reflection loss on the surface of the shielding material, and  $SE_M$  is multiple reflection loss inside the shielding material. These parameters are written as:

$$SE_A = 131.43t\sqrt{f\mu_r\sigma_r}, \quad (3)$$

$$SE_R = 20 \log\left(5.35r\sqrt{\frac{f\sigma_r}{\mu_r}} + 0.354 + \frac{1.17 \times 10^{-2}}{r} \sqrt{\frac{\mu_r}{f\sigma_r}}\right), \quad (4)$$

$$SE_M = 10 \log(1 - 2 \times 10^{-0.1 \times SE_A} \times \cos(0.23SE_A) + 10^{-0.2 \times SE_A}). \quad (5)$$

$t$  is the thickness of the shielding in meters,  $r$  is the distance between the EMF source and the shielding plates in meters,  $\mu_r$ ,  $\sigma_r$  are the relative permeability and the corresponding electrical conductivity, respectively. If  $SE_A$  is greater than 15 dB,  $SE_M$  comparably is very small; and thus it can be negligible value. In general, the single reflection loss of the most materials is minimal; therefore, the  $SE$  can be approximated equal to  $SE_A$ .

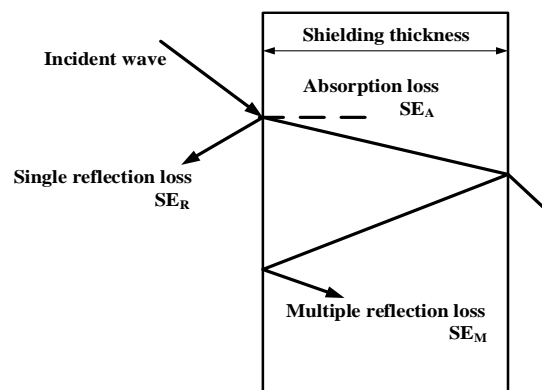


Figure 5. Electromagnetic wave behavior inside and outside of the shielding materials.

### 3. Systems Model and Analysis

In this section, three types of shielding models and analysis are discussed. FEM software solver is used to analyze and compare the effects of shielding techniques on the WPT system power transfer efficiency (based on the coupling coefficient), and the system inductances for the two coil circular pad WPT system when using a fixed operating frequency for the series-series (SS) compensation topology. The lumped circuit model which presented in Ref. [33] is used for the ferrite and aluminum shielding, while the circuit model for the resonant reactive current shield is discussed in this section. The power source internal resistance and the load resistance are selected to be  $50 \Omega$  and  $10 \Omega$ , respectively.

#### 3.1. WPT System Model in the Presence of Ferrite Shielding

When adding ferromagnetic material to Tx or/and Rx coils that will increase the analysis complexity due to the nonlinear behavior, which comes from the influence of the hysteresis and eddy current losses. Materials generally respond to an applied magnetic field  $H$  with a change in their magnetic dipole moments  $P_m$ . Therefore, the macroscopic magnetic dipole density or simply, a magnetization  $M$  can be given as [34]:

$$M = \chi_m H. \quad (6)$$

$\chi_m$  is the magnetic susceptibility, which is dimensionless proportionality constant that indicates the degree of magnetization of a material in response to an applied field [35]. The relation between  $B$ ,  $H$ , and  $M$  is through the material permeability  $\mu = \mu_0\mu_r$ , with free space permeability  $\mu_0 = 4\pi \times 10^{-7} \text{H/m}$ , and  $\mu_r$  is the ratio of the specific material permeability to the free space permeability called relative permeability:

$$\begin{aligned} B &= \mu_0(H + M) = \mu_0(H + \chi_m H) = \mu_0 H(1 + \chi_m) \\ &= \mu_0 \mu_r H = \mu H. \end{aligned} \quad (7)$$

The magnetic flux density  $B$  includes both the external field  $\mu_0 H$ , and the material response  $\mu_0 M$ . Therefore, the WPT model in the presence of ferromagnetic material can be as that discussed in [36].

For the analysis, the FEM software solver is used to implement how the ferromagnetic materials can affect the WPT system design. Firstly, circular coils are used only without ferrite cores; secondly, two iron cores are added to the same coils as depicted in Figure 6.

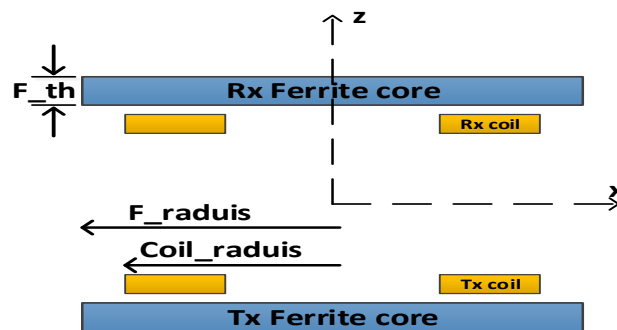


Figure 6. Wireless power transfer (WPT) system pad structure in the presence of ferrite cores.

The simulation parameters are presented in Table 1.

Table 1. The simulation design parameters.

Parameters	Value	Description
The WPT coil radius	20 cm	Litz wire $\varphi = 3.5$ mm
The ferrite core radius	22.5 cm	$\mu_r = 4000, 10.3 \times 10^6$ S/m
Ferrite core thickness (F-th)	3 mm	-
WPT coils Number of turns	20 turns	-
Air gap (d)	15 cm	-
Operating frequency	85 kHz	-
Power transfer	500 W	-

Power transfer efficiency is plotted for different frequencies for the two coils only and compared to the design when adding ferrite cores to the Tx and Rx coils as depicted in Figure 7 for SS design with load resistance  $10 \Omega$ . In this case, the compensation capacitors are remaining the same as in design without cores; therefore, the resonant frequency is changed. From this figure, it is clear that the WPT system is susceptible to the ferromagnetic materials. Accordingly, the system needs to readjust the capacitors or the operating frequency automatically. Moreover, adding ferrite cores improves the system efficiency from about 60% to about 78%. Readjusting the compensation capacitors after adding the ferrite cores can increase the system performance and lets the system resonate at the operating frequency as depicted in Figure 8.

The leakage magnetic flux also is reduced, which will increase the magnetic coupling. The XY measure plane ( $60 \text{ cm} \times 60 \text{ cm}$ ) above the secondary coil by 10 cm can give sense more than using shielding effectiveness to compare the magnetic field intensity (A/m) for the coils only and the coils

with magnetic shielding as presented in Figure 9a,b. It is clear that the magnetic shield has good shield effectiveness because the leakage is significantly reduced because the magnetic plates guide the magnetic flux along and inside the plates [37].

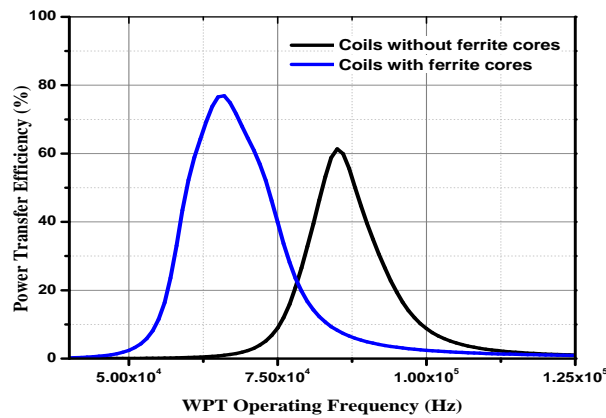


Figure 7. Power transfer efficiency in the absence and the presence of ferrite cores after readjusting the capacitors.

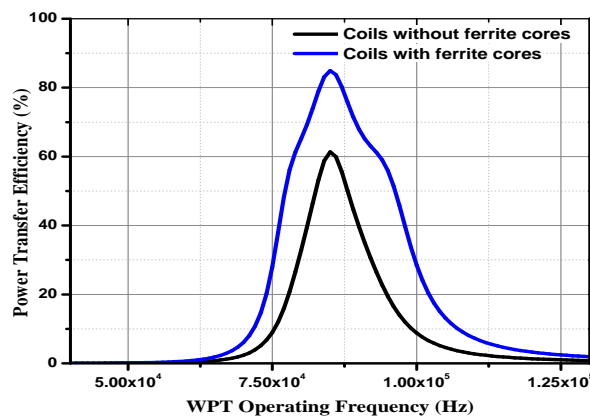


Figure 8. Power transfer efficiency in the absence and the presence of ferrite cores after readjusting the capacitors.

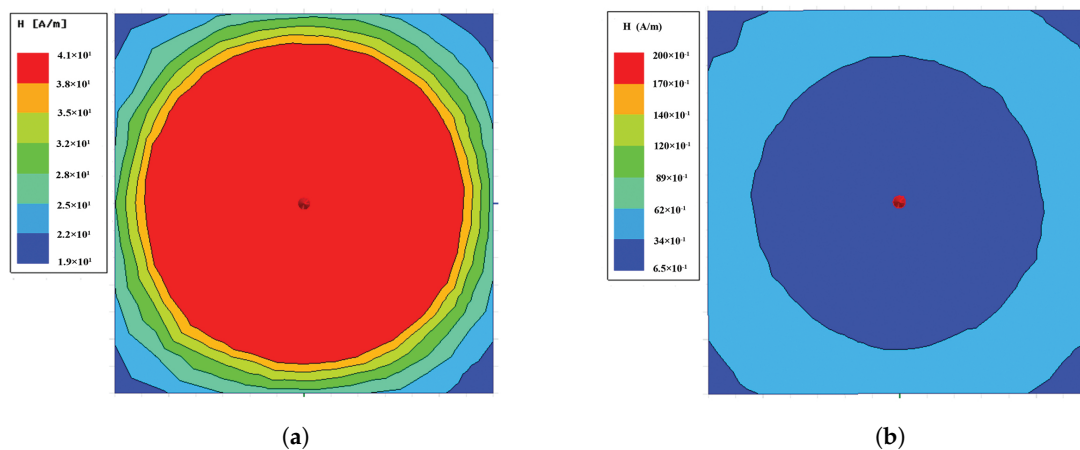


Figure 9. Magnetic field intensity (A/m), (a) two coils w/o ferrite core; (b) two coils with ferrite cores.

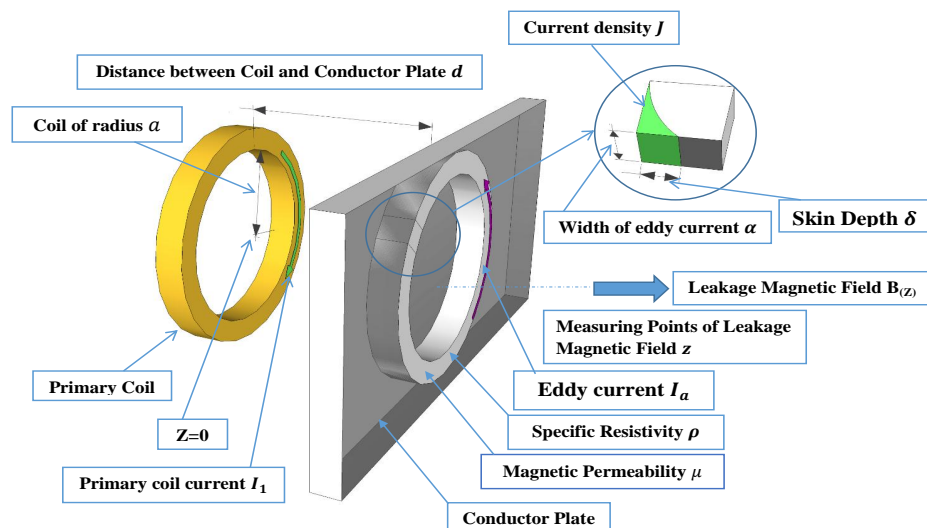
Table 2 presents the self- and mutual inductances and other simulation results for the two coils and the two coils with the ferrite cores. From this table, it can be observed that the ferrite cores can increase the self- and mutual inductances and thus will increase the coupling coefficient. Moreover, adding a magnetic core can decrease the current stress on the primary coils for the same power transfer.

**Table 2.** The simulation design results for coils and coils with cores.

Parameters	Coils Only	Coils with Ferrite Cores
Tx Self-inductance ( $\mu\text{H}$ )	210.1	360.11
Rx Self-inductance ( $\mu\text{H}$ )	212.96	360.6
Mutual inductance ( $\mu\text{H}$ )	33.611	77.718
The coupling coefficient	0.158	0.216
Primary current (A)	12.43	5.38
Secondary current (A)	4.47	4.47

### 3.2. WPT Modeling in the Presence of Metallic Shield

A simple and effective way to reduce the leakage flux in WPT environments is to use metallic plates with the Tx and Rx coils. The eddy current induced in these plates produces a magnetic field opposes that flux generated by the WPT coils. The WPT system in the presence of metallic material (aluminum) is presented in Figure 10 using one side to describe the change in magnetic flux density in this case. Figure 10 shows the one turn excited coil, and the eddy current flows in the metal plate as a mirror of current in the WPT coil and in the opposite direction [38].

**Figure 10.** WPT approximation model in the presence of metallic materials.

The magnetic flux density produced by the excited coil  $B_1(T)$  can be given as:

$$B_1 = \frac{\mu_0 a^2}{2(a^2 + z^2)^{\frac{3}{2}}} I_1. \quad (8)$$

The magnetic flux density produced by the eddy current (mirror loop)  $B_2(T)$  can be given as:

$$B_2 = -\frac{\mu_0 a^2}{2(a^2 + (z-d)^2)^{\frac{3}{2}}} \frac{j\omega M}{R_a + j\omega L_a} I_1. \quad (9)$$

Then, the total magnetic flux density is:

$$B = B_1 + B_2. \quad (10)$$

$M$  represents the mutual inductance between the coil and the eddy current in the shielding plate given by:

$$M = \mu_o a \left( \log \frac{8a}{d} - 2 \right). \tag{11}$$

$L_a, R_a$  are the self-inductance and the total resistance of the eddy current circuit respectively. In addition, it can be given as follows:

$$L_a = a \left( \mu_o \left( \log \frac{8a}{r} - 2 \right) + \frac{\mu_o}{4} \right), \tag{12}$$

where  $r$  is the wire radius.

$$R_a = \frac{2\pi a}{\alpha \delta}, \tag{13}$$

where  $\alpha$  is the width of the eddy current, and  $\delta$  is the skin depth and given as

$$\delta = \sqrt{\frac{\rho}{\pi f \mu}}. \tag{14}$$

$\rho$  is the conductor resistivity,  $f$  is operating frequency, and  $\mu$  is the magnetic permeability.

FEM solver is used to evaluate and compare the electromagnetic environment and the system performance for WPT system with ferrite cores only as discussed in Section 1 and with ferrite cores with aluminum shielding plates as shown in Figure 11. The simulation parameters are presented in Table 3.

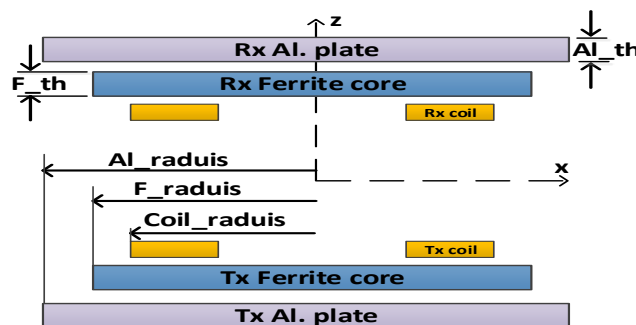


Figure 11. WPT system pad structure in the presence of ferrite cores and Al plates.

Table 3. The simulation design parameters.

Parameters	Value	Description
The WPT coil radius	20 cm	Litz wire $\varphi = 3.5$ mm
The ferrite core radius	22.5 cm	$\mu_r = 4000; 10.3 \times 10^6$ S/m
The ferrite core thickness (F-th)	3 mm	-
Al plates radius	30 cm	$\mu_r = 1; 10.3 \times 10^6$ S/m
Al plate thickness (Al-th)	3 mm	-
The WPT coil Number of turns	20 turns	-
Air gap (d)	15 cm	-
Operating frequency	85 kHz	-
Power transfer	500 W	-

The system performance is compared for the two designs as in Figure 12; it is clear that adding metallic shielding plates leads to reducing the system performance and changing the system parameters. For evaluating the electromagnetic environment, the XY measure plane is used to present the electromagnetic field intensity as illustrated in Figure 13. From Figure 13, it is proved that

using the metallic shield effectively reduces the EMF above the secondary coil where is the driver may be presented.

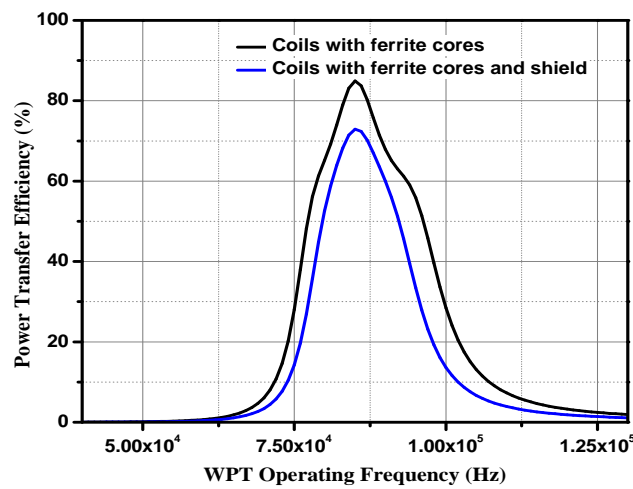


Figure 12. System performances for coils with ferrite cores and with ferrite and Al plates.

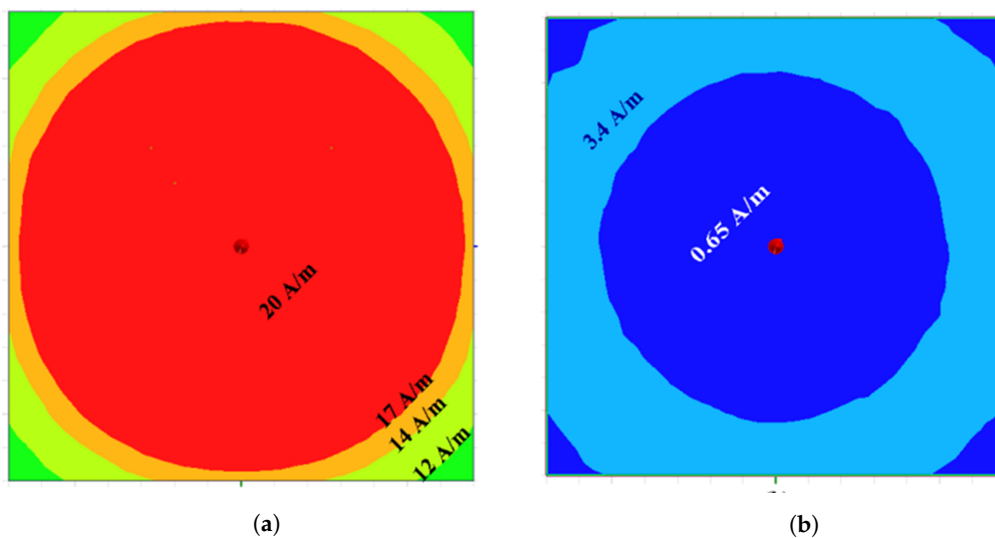


Figure 13. Magnetic field intensity (A/m), (a) two coils with ferrite core; (b) two coils with ferrite cores and Al plates.

Table 4 shows the simulation results for the coils with cores compared to the coils with cores and with the conductive plates. From this table, it is clear that the self- and mutual inductances are decreased when using aluminum plates. Moreover, the secondary current is increased due to the eddy currents generated in the Al plates.

Table 4. The simulation design results for coils with ferrite and coils with core and shields.

Parameters	Coils with Ferrite	Coils with Ferrite and Al
Tx Self-inductance ( $\mu\text{H}$ )	360.11	328.96
Rx Self-inductance ( $\mu\text{H}$ )	360.6	329.61
Mutual inductance ( $\mu\text{H}$ )	77.718	53.64
The coupling coefficient	0.216	0.163
Primary current (A)	5.38	7.81
Secondary current (A)	4.47	4.47

### 3.3. WPT System Model for Resonant Reactive Current (RRC) Shielding

The WPT system equivalent circuit using the lumped parameters model when the RRC shield is used for the SS WPT system can be presented as the four coils WPT system as in Figure 14.

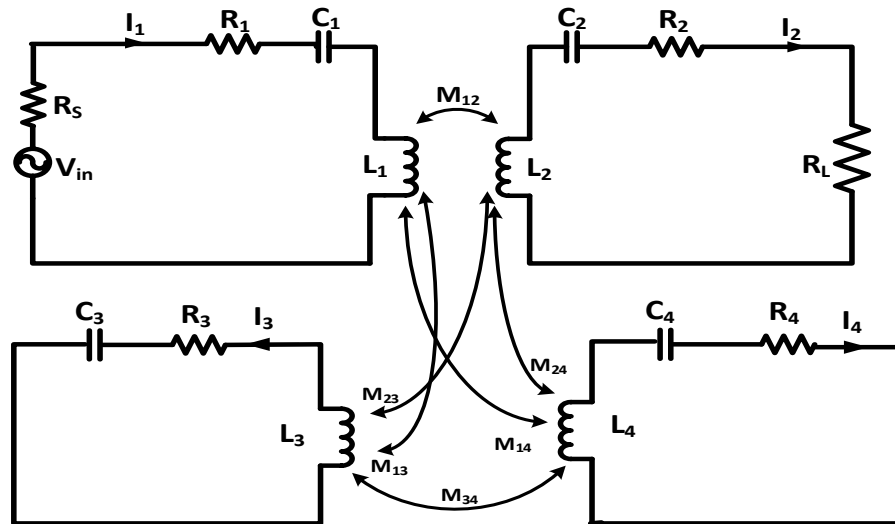


Figure 14. WPT system with the resonant reactive current shielding equivalent circuit model.

$I_{1,2}$ ,  $R_{1,2}$ ,  $C_{1,2}$ , and  $L_{1,2}$  are the currents, resistances, capacitors, and inductances for Tx and Rx coils, respectively.  $I_{3,4}$ ,  $R_{3,4}$ ,  $C_{3,4}$ , and  $L_{3,4}$  are the corresponding parameters for the Tx shielding and Rx shielding loops, respectively.  $V_{in}$ ,  $R_s$ , and  $R_L$  are the RMS value for the power source, the power source internal resistance ( $50 \Omega$ ), and the equivalent load resistance, respectively. While  $M_{12}$ ,  $M_{13}$ ,  $M_{14}$ ,  $M_{23}$ ,  $M_{24}$ ,  $M_{34}$  presented the mutual inductances between the four coils as shown in Figure 14. The system impedance matrix can be written as:

$$\begin{pmatrix} Z_{11} & Z_{12} & Z_{13} & Z_{14} \\ Z_{21} & Z_{22} & Z_{23} & Z_{24} \\ Z_{31} & Z_{32} & Z_{33} & Z_{34} \\ Z_{41} & Z_{42} & Z_{43} & Z_{44} \end{pmatrix} \begin{pmatrix} I_1 \\ I_2 \\ I_3 \\ I_4 \end{pmatrix} = \begin{pmatrix} V_{in} \\ 0 \\ 0 \\ 0 \end{pmatrix}, \quad (15)$$

where  $Z_{nn} = R_{nn} + j\omega L_{nn} + 1/j\omega C_{nn}$ , and  $Z_{mn} = j\omega M_{mn}$ ,  $(m, n) \in (1, 2, 3, 4)$ , and  $R_{11} = R_1 + R_s$ ,  $R_{22} = R_2 + R_L$ .

Matching capacitors are added to Tx and Rx shielding loops to control the magnitude and phase for the current induced in the shielding loops. Currents induced in shielding loops depend on the loop impedances and the voltage induced ( $V_{ind}$ ); therefore, current in the shielding loops can be described as in Equation (16):

$$\begin{aligned} I_{sh1,2} &= \frac{V_{ind}}{Z_{sh1,2}} \\ &= \frac{V_{ind}}{R_{sh1,2} + j\omega L_{sh1,2} + 1/j\omega C_{sh1,2}}. \end{aligned} \quad (16)$$

Controlling the shielding loop impedance is the key factor in designing resonant reactive current shield, which determines the phase and magnitude of the current in the shielding loop and hence determines the phase and amplitude of the generated canceling magnetic field. Then, added capacitors are used to define the resonance frequency and impedance of the shielding loops. The magnitude and phase of the shielding loop impedance are presented in Figure 15. To keep the shielding impedance as

low as possible and the phase at  $90^\circ$ , the system must resonate at the inductive region. In this case, the canceling magnetic field is in the opposite direction to the WPT magnetic field [26], which leads to enhancing the system performance and the shielding effectiveness compared to the non-resonant shielding [39]. The system operating frequency is 85 kHz, and is located here in the inductive region when the shielding is resonating at 80 kHz. Thereby, the shielding impedance is a fraction and the phase at  $90^\circ$ . However, the current in the shielding loop must be carefully adjusted, and thick shielding coils may be needed at the low impedance case.

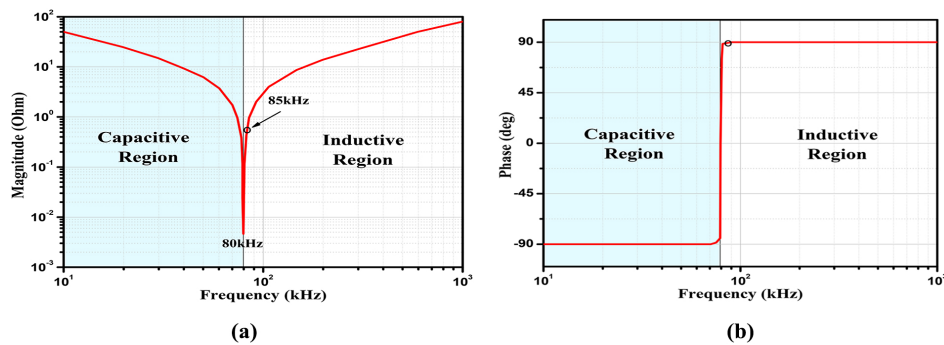


**Figure 15.** Resonant reactive shield impedance; (a) impedance magnitude; and (b) impedance phase.

### 3.3.1. The Loop Position in RRC Shielding

Firstly, the RRC shielding loop position is investigated, and the EMF environment surrounding the design is observed and compared for the two proposed positions. The first position, the loops located surrounding the WPT coils and on the same level as the WPT coils (case 1) are shown in Figure 16a. Secondly, the loops placed above and under the ferrite cores have the same radius of loops in case1 (case 2) as shown in Figure 16b, and the two cases have the same parameters.

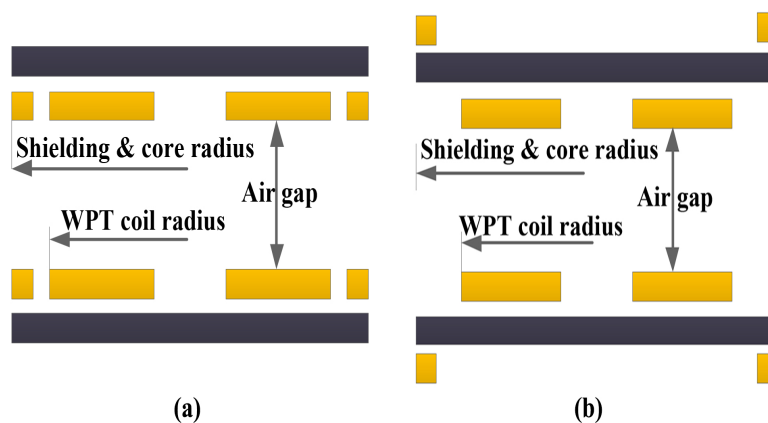


**Figure 16.** The proposed shielding loop positions; (a) the two loops on the same levels with the WPT coils, and (b) the two loops located above and under the ferrite cores.

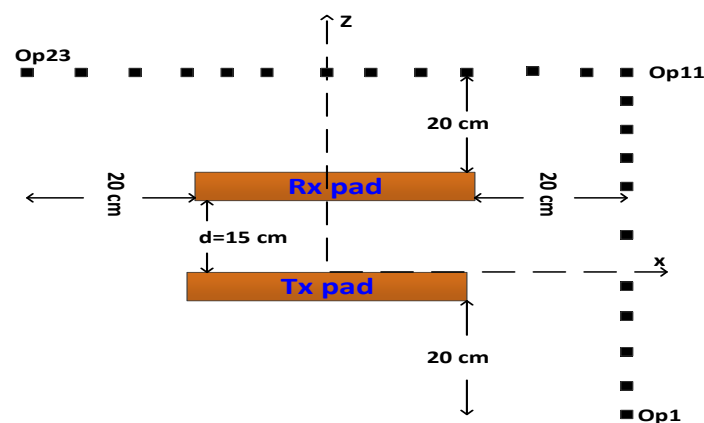
Using the finite element method (FEM) software to investigate the environment surrounding the design, the two designs are simulated using the same parameters as in Table 5. The operating frequency is 85 kHz. The WPT system is tested for transferring 5 kW.

**Table 5.** The design parameters of the Resonant Reactive Current (RRC) shielding loop position.

Parameters	Value	Description
The ferrite core radius	22.5 cm	$\mu_r = 4000 ; 10.3 \times 10^6 \text{ S/m}$
The shielding loop radius	22.5 cm	Litz wire $\varphi = 3.5 \text{ mm}$
The WPT coil radius	20 cm	Litz wire $\varphi = 3.5 \text{ mm}$
The ferrite core thickness	5 mm	-
RRC loop Number of turns	3 turns	-
WPT coil Number of turns	20 turns	-
Air gap	15 cm	-

### 3.3.2. EMF Environment Evaluation Method

This section is inspired by the three-point measurement procedure for public EMF exposure, which is introduced by international standard IEC-62110 [40]. Observation points' configurations are arranged in the  $z$ -axis (from Op1–Op11) where the people on the pedestrian can be presented, and on the  $x$ -axis (from Op11–Op23) where the EV driver can be located as depicted in Figure 17. This method is active when comparing the simulation results with the measured one. Since the design is symmetric, these two axes are enough to test the electromagnetic field surrounding the design.

**Figure 17.** Observation points configurations for testing the Electromagnetic Field (EMF) level on the  $x$  and  $z$ -axes.

### 3.3.3. Simulation Results for the Two Proposed Shielding Loop Positions

Using FEM software (ANSYS Maxwell 16, ANSYS, Inc., Canonsburg, PA, USA), the two proposed shielding position designs are simulated when the solution is eddy current. EMF levels at the observation points are recorded and compared when the power transferred is 5 kW. Figure 18a presented the EMF level curves for the two proposed designs for the  $z$ -axis observation points, while the  $x$ -axis observation EMF values are depicted in Figure 18b. From these figures, it is clear that when the two shielding loops are located on the same level of the WPT coils, the magnitude of the EMF for the  $z$  and  $x$ -axes are significantly reduced. Figure 19a,b presents the magnetic flux density distributions on the side view for case 1 and case 2, respectively. From these figures, it is proved that the design in case 1 succeeds at reducing the EMF surrounding the charger.

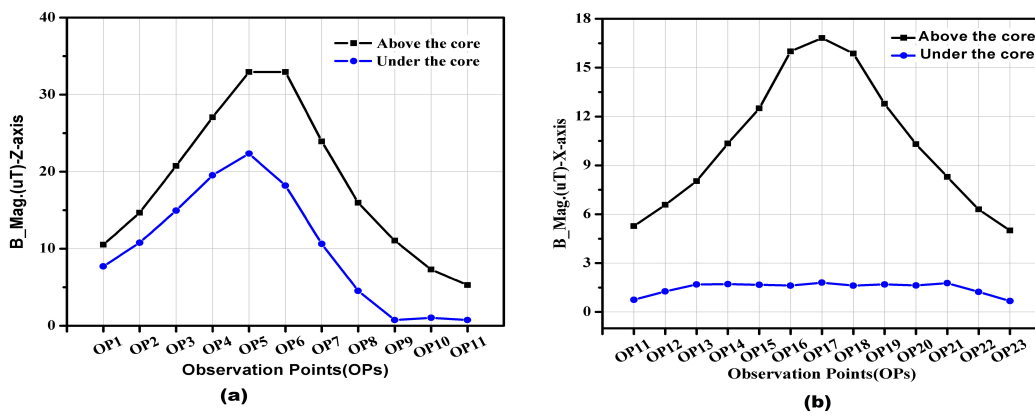


Figure 18. The EMF level for the two proposed designs observed on (a) z-axis points and (b) x-axis points.

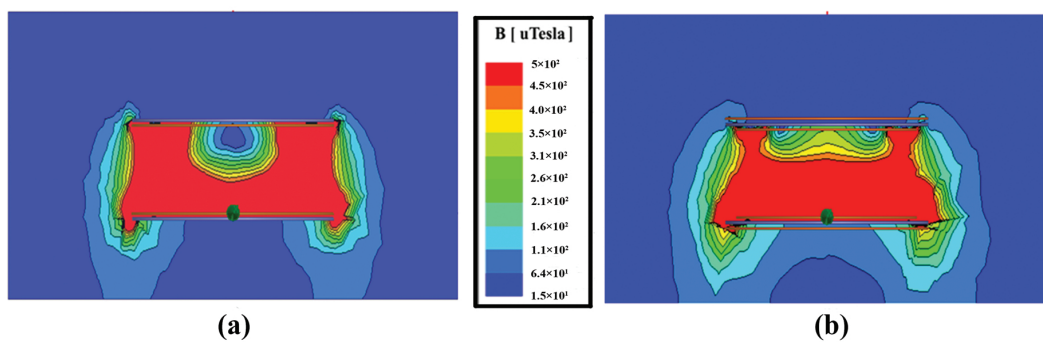


Figure 19. Magnetic flux distributions for side plane ( $\mu\text{T}$ ); (a) case 1 and (b) case 2.

#### 4. The Proposed Shielding Techniques

In this section, the three shielding techniques discussed in Section 3 are investigated using the FEM solver and prototypes are also built to transfer 5 kW through 15 cm. The electromagnetic environment is extensively evaluated and compared using the method introduced in Section 3.3.2. EMF levels are tested along  $x$  and  $z$ -axes to compare the average of EMF levels between the three proposed shielding techniques. The charger pad weight also is considered and compared for dimensions and materials specifications as reported in Table 6.

Table 6. The proposed shielding techniques’ design parameters.

Parameters	Value	Specifications
WPT coil loop radius	20 cm	Litz wire $\varphi = 3.5 \text{ mm}$ ; $5.8 \times 10^7 \text{ S/m}$ ; $8933 \text{ kg/m}^3$
WPT coil number of turns	20 turns	-
Ferrite core radius	22.5 cm	$\mu_r = 4000$ ; $10.3 \times 10^6 \text{ S/m}$ ; $7870 \text{ kg/m}^3$
Ferrite core thickness	0.5 cm	-
Al shield thickness	0.5 cm	-
Al shield radius	25 cm	$3.8 \times 10^7 \text{ S/m}$ ; $2689 \text{ kg/m}^3$
The reonant loop radius	22.5 cm	-
The resonant shield number of turns	3 turns	-
Air-gap	15 cm	-
Operating frequency	85 kHz	-
Power transfer	5 kW	-

##### 4.1. Simulation Results and Analysis

EMF is considered for the all observation points and the averages for the  $z$ -axis and  $x$ -axis are calculated and compared as shown in Table 7. The operating frequency is fixed to 85 kHz, and power

transferred to the load is 5 kW. From this table, we can observe that the resonant reactive current shield succeeds at reducing about 81% and 95% of the EMF average for the z-axis and x-axis, respectively, while the Al-shield reduced about 71% and 64% for z-axis and x-axis of the EMF average, respectively; all these values were compared to the ferrite shielding technique.

**Table 7.** Electromagnetic Field (EMF) averages for z-axis and x-axis observation points.

The Shielding Type	z-Axis EMF	%	x-Axis EMF	%
Ferrite shield	49.30	100%	34.12	100%
Al shield	28.63	58.07%	12.32	36.10%
Resonant shield	9.15	18.60%	1.56	4.60%

The comparison between the self-inductance and mutual inductance for the three proposed cases are presented in Table 8. According to the relation between the coupling coefficient and inductances, it is clear that the resonant reactive current shielding has a high system performance among the others based on the coupling coefficient. Moreover, the Al-shielding reduced about 7.3% and 15% of the self-inductance and mutual inductance, respectively, compared to the resonant reactive current shielding.

**Table 8.** The inductances comparison for the proposed causes.

The Shielding Type	$L_1$ ( $\mu$ T)	%	$L_2$ ( $\mu$ T)	%	$M$ ( $\mu$ T)	%
Ferrite shield	348.94	99.8%	349.45	99.8%	76.14	99.5%
Al shield	324.08	92.7%	324.16	92.6%	57.33	74.9%
RRC shield	349.59	100%	350.22	100%	76.54	100%

In designing a WPT charger, the weight is a critical factor. For a comparison between the three proposed shielding techniques, the total weight for the charger's pads is depicted in Figure 20, where:

- ferrite shield total weight includes the two WPT coils plus the two ferrite cores,
- aluminum shield total weight includes the two WPT coils plus the two ferrite cores plus the two aluminum plates,
- resonant reactive current shield total weight includes the two WPT coils plus the two ferrite cores plus the two resonant loops weight.

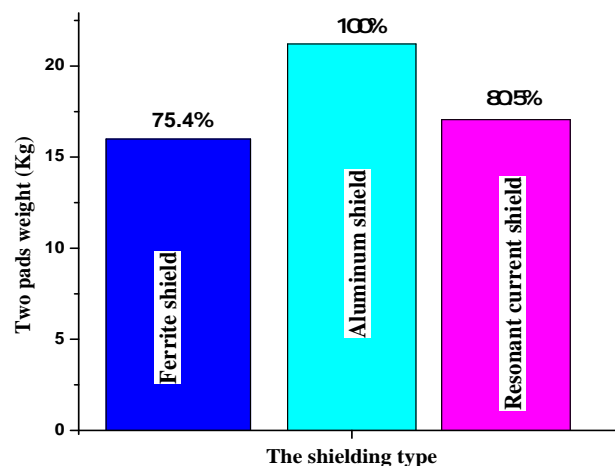


**Figure 20.** The total pad weight for the three proposed shielding techniques.

From Figure 20, Tables 7 and 8, we can see that the ferrite shield design is lightweight and has good performance; however, the EMF leakage is very high. Contrary to the ferrite shield is the aluminum shield, which has a heavy weight and bad system performance. While the resonant reactive current shield has a high system performance, and is lightweight compared to the aluminum shield. Moreover, the resonant current shield gained a minimum EMF leakage compared to the other shielding techniques.

The magnetic flux density ( $\mu\text{T}$ ) distribution in the YZ plane for the ferrite, aluminum, and resonant reactive current shields are presented in Figure 21. A vertical line located 45 cm away from the coils center and a horizontal line located 6 cm above the secondary coil used as observation lines. It is evident from Figure 21c that the resonant reactive current shielding has less EMF leakage surrounding the WPT charger.

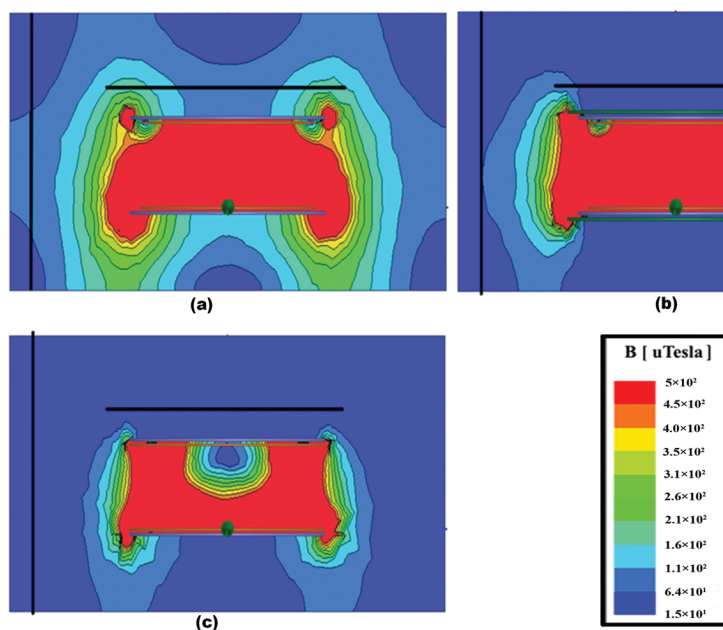


**Figure 21.** The magnetic flux density distribution ( $\mu\text{T}$ ), (a) is the ferrite shield; (b) is the aluminum shield; and (c) is the resonant reactive current shield.

#### 4.2. The Experimental Set-Up

In this part, the experiment is set up as shown in Figure 22 to validate the simulation results. SS compensation topology is used, and LCR meter 3522-50 LCR HiTESTER (Hioki E.E. Corporation, Nagano city, Japan) is used to measure the inductances and resistances of the coils. Prototypes are built to transfer 5 kW through a 15 cm air gap.

The magnetic flux density (B-Mag) levels are measured for  $x$  and  $z$ -axes' observation points (refer to Figure 17) for the three types of shielding techniques and compared to the simulation one. Narda HP032 EMF probe (Narda, Segrate, Italy) is used for measuring the EMF level. The observation points are arranged 20 cm away from the edge of the coils to give 11 points on the  $z$ -axis as discussed before, and the comparison of the EMF levels for the simulation and the measurement are depicted in Figure 23. The  $x$ -axis observation points are arranged 20 cm above the secondary coil in the  $x$ -axis direction because the design is symmetric for the  $x$ - and  $y$ -axes. The comparison between the measured and simulated results for the  $x$ -axis for the three shielding techniques are presented in Figure 24.

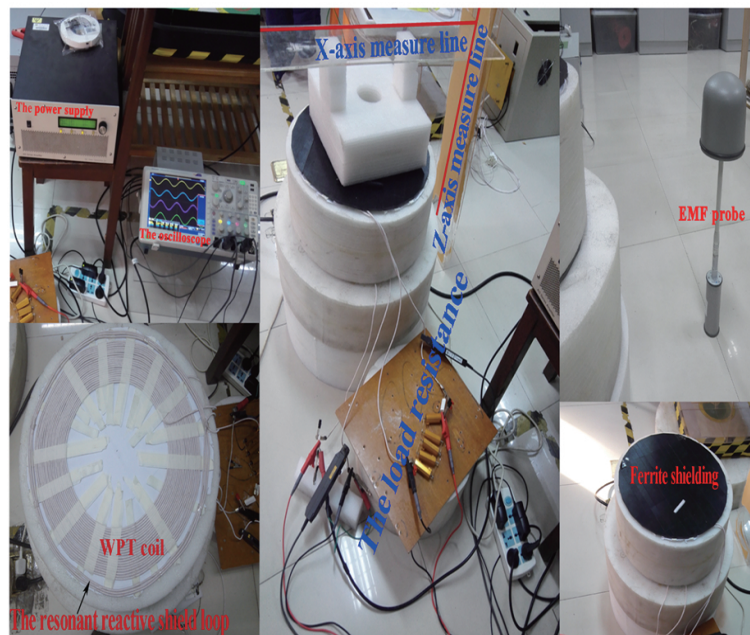


Figure 22. The experimental set-up.

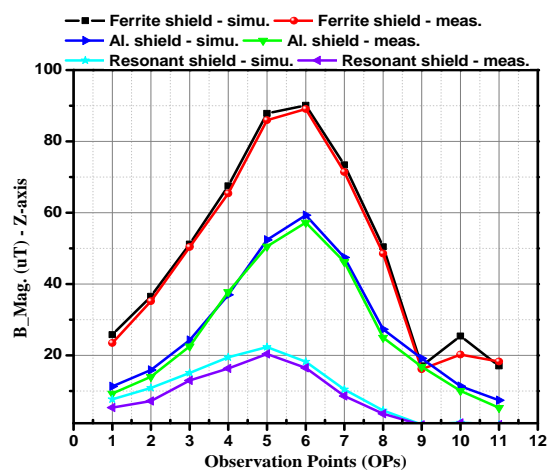


Figure 23. Measurement and simulation B-Mag ( $\mu\text{T}$ ) on the z-axis for the three shielding types.

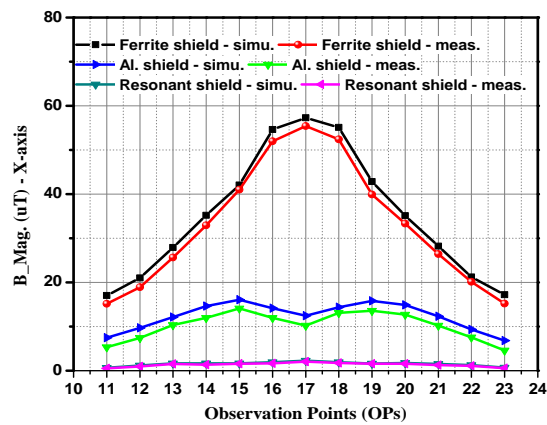


Figure 24. Measurement and simulation B-Mag ( $\mu\text{T}$ ) on the x-axis for the three shielding types.

From Figures 23 and 24, it is clear that the resonant reactive current shielding technique gained the minimum EMF level compared to the other proposed shielding techniques. Moreover, the measured and simulated results are well matched.

## 5. Conclusions

In this paper, shielding techniques used in WPT systems for charging EVs are investigated. Magnetic, metallic, and resonant reactive current shielding are intensively discussed and compared based on the EMF level, system performance, and the total charger's weight. Circular coils and cores are used with the circular Al plates for conventional shielding as well as with the resonant reactive current shield to transfer 5 kW through 15 cm air gap for 85 kHz fixed operating frequency. Shielding effectiveness and how shielding materials may affect the system performance and other parameters such as inductances are precisely analyzed. The results of the analysis show that adding magnetic materials will improve the system efficiency and it can orient most parts of the magnetic leakage flux. However, the compensation capacitors or the system operating frequency need to be readjusted. Although adding metallic materials will reduce the system performance, it can also significantly reduce the EMF level. The resonant reactive current shield gained acceptable system efficiency as well as reducing the EMF level more than the metallic materials. However, the shielding loop position and the shielding impedance need to be carefully designed. Therefore, the shielding loop position is investigated and the results show that when the loop is on the same level as the WPT coils under the magnetic core, the EMF level is significantly reduced. Moreover, controlling the shielding impedance is also discussed.

The EMF evaluation method used in this study can be applied for evaluating the EMF environment surrounding any other high frequency devices. The EMF environment surrounding the chargers is extensively evaluated and compared. Simulation and measurement results for the three proposed shielding types are compared; the results show that the simulation and practical values are well matched. In the future, the optimum design for each proposed shielding technique can be compared.

**Author Contributions:** L.T. and K.E. conceived the concept and designed the models for simulation; L.T., H.X. and M.J. derived the models and analyzed the data; K.E. and M.J. performed the experiments; H.X. and K.E. managed the resources. K.E. supervised the work. All authors contributed in writing the manuscript.

**Funding:** This work was supported by the National Key R&D project (No.2018YFB0106300).

**Conflicts of Interest:** The authors declare no conflict of interest.

## References

1. An, F. CHAPTER 9—International Comparison of Policies to Reduce Greenhouse Gas Emissions from Passenger Vehicles. In *Driving Climate Change*; ELSEVIER Inc.: Burlington, VT, USA, 2007; pp. 143–164.
2. Wang, H.; Hasanzadeh, A.; Khaligh, A. Transportation Electrification: Conductive charging of electrified vehicles. *IEEE Electr. Mag.* **2013**, *1*, 46–58. [[CrossRef](#)]
3. Yilmaz, M.; Krein, P.T. Review of battery charger topologies, charging power levels, and infrastructure for plug-in electric and hybrid vehicles. *IEEE Trans. Power Electron.* **2013**, *28*, 2151–2169. [[CrossRef](#)]
4. Khaligh, A.; Dusmez, S. Comprehensive topological analysis of conductive and inductive charging solutions for plug-in electric vehicles. *IEEE Trans. Veh. Technol.* **2012**, *61*, 3475–3489. [[CrossRef](#)]
5. Villa, J.L.; Sallán, J.; Llombart, A.; Sanz, J.F. Design of a high frequency inductively coupled power transfer system for electric vehicle battery charge. *Appl. Energy* **2009**, *86*, 355–363. [[CrossRef](#)]
6. Throngnumchai, K.; Kai, T.; Minagawa, Y. A study on receiver circuit topology of a cordless battery charger for electric vehicles. In Proceedings of the 2011 IEEE Energy Conversion Congress and Exposition, Phoenix, AZ, USA, 17–22 September 2011.
7. Wang, C.-S.; Stielau, O.H.; Covic, G. Design considerations for a contactless electric vehicle battery charger. *IEEE Trans. Ind. Electron.* **2005**, *52*, 1308–1314. [[CrossRef](#)]
8. Campi, T.; Cruciani, S.; Feliziani, M. Wireless power transfer technology applied to an autonomous electric UAV with a small secondary coil. *Energies* **2018**, *11*, 352. [[CrossRef](#)]

9. Guideline, I. Guidelines for limiting exposure to time-varying electric, magnetic, and electromagnetic fields (up to 300 GHz). *Health Phys.* **1998**, *74*, 494–522.
10. International Commission on Non-Ionizing Radiation Protection. Guidelines for limiting exposure to time-varying electric and magnetic fields (1 Hz to 100 kHz). *Health Phys.* **2010**, *99*, 818–836.
11. IEEE Standards Coordinating Committee. *IEEE Standard for Safety Levels with Respect to Human Exposure to Radio Frequency Electromagnetic Fields, 3 kHz to 300 GHz*; IEEE C95. 1-1991; IEEE Standards Board: New York, NY, USA, 1992.
12. Elnail, K.; Huang, X.; Xiao, C.; Tan, L.; Haozhe, X. Core structure and electromagnetic field evaluation in wpt systems for charging electric vehicles. *Energies* **2018**, *11*, 1734. [[CrossRef](#)]
13. Kim, H.; Song, C.; Kim, J.; Kim, J.; Kim, J. Shielded coil structure suppressing leakage magnetic field from 100 W-class wireless power transfer system with higher efficiency. In Proceedings of the 2012 IEEE MTT-S International Microwave Workshop Series on Innovative Wireless Power Transmission: Technologies, Systems, and Applications, Kyoto, Japan, 10–11 May 2012.
14. Ahn, S.; Hwang, C.; Park, H.H. Optimized shield design for reduction of EMF from wireless power transfer systems. *IEICE Electron. Express* **2014**, *11*, 20130930. [[CrossRef](#)]
15. Ogawa, K.; Oodachi, N.; Obayashi, S.; Shoki, H. A study of efficiency improvement of wireless power transfer by impedance matching. In Proceedings of the 2012 IEEE MTT-S International Microwave Workshop Series on Innovative Wireless Power Transmission: Technologies, Systems, and Applications, Kyoto, Japan, 10–11 May 2012.
16. Feliziani, M.; Cruciani, S. Mitigation of the magnetic field generated by a wireless power transfer (WPT) system without reducing the WPT efficiency. In Proceedings of the 2013 International Symposium on Electromagnetic Compatibility, Brugge, Belgium, 2–6 September 2013.
17. Kim, J.; Kim, J.; Kong, S.; Kim, H.; Suh, I.S.; Suh, N.P.; Cho, D.H.; Kim, J.; Ahn, S. Coil design and shielding methods for a magnetic resonant wireless power transfer system. *Proc. IEEE* **2013**, *101*, 1332–1342. [[CrossRef](#)]
18. Kim, H.; Song, C.; Kim, J. Coil design for high efficiency and low magnetic field leakage of wireless charging system for electric vehicle. In Proceedings of the 2015 IEEE Wireless Power Transfer Conference (WPTC), Boulder, CO, USA, 13–15 May 2015.
19. Campi, T.; Cruciani, S.; Feliziani, M. Magnetic shielding of wireless power transfer systems. In Proceedings of the 2014 International Symposium on Electromagnetic Compatibility, Tokyo, Japan, 12–16 May 2014.
20. Ahn, S.; Kim, J. Magnetic field design for high efficient and low EMF wireless power transfer in on-line electric vehicle. In Proceedings of the European Conference on Antennas & Propagation, Rome, Italy, 11–15 April 2011.
21. Lee, S.; Lee, W.; Huh, J.; Kim, H.J.; Park, C.; Cho, G.H.; Rim, C.T. Active EMF cancellation method for I-type pickup of On-Line Electric Vehicles. In Proceedings of the 2011 Twenty-Sixth Annual IEEE Applied Power Electronics Conference and Exposition (APEC), Fort Worth, TX, USA, 6–11 March 2011.
22. Townsend, L.W. Critical analysis of active shielding methods for space radiation protection. In Proceedings of the 2005 IEEE Aerospace Conference, Big Sky, MT, USA, 5–12 March 2005.
23. Jonsson, U.; Larsson, A.; Sjodin, J.O. Optimized reduction of the magnetic field near Swedish 400 KV lines by advanced control of shield wire currents. Test results and economic evaluation. *IEEE Trans. Power Deliv.* **1994**, *9*, 961–969. [[CrossRef](#)]
24. Moon, H.; Ahn, S.; Chun, Y. Design of a novel resonant reactive shield for wireless charging system in electric vehicle. In Proceedings of the in 2014 IEEE Wireless Power Transfer Conference, Jeju, Korea, 8–9 May 2014.
25. Moon, H.; Kim, S.; Park, H.H.; Ahn, S. Design of a resonant reactive shield with double coils and a phase shifter for wireless charging of electric vehicles. *IEEE Trans. Magn.* **2015**, *51*, 1–4. [[CrossRef](#)]
26. Kim, S.; Park, H.H.; Kim, J.; Kim, J.; Ahn, S. Design and analysis of a resonant reactive shield for a wireless power electric vehicle. *IEEE Trans. Microw. Theory Tech.* **2014**, *62*, 1057–1066. [[CrossRef](#)]
27. Elnail, K.E.I.; Huang, X.; Tan, L. Optimal resonance reactive current shielding design in wireless power transfer systems. In Proceedings of the 2017 China International Electrical and Energy Conference (CIEEC), Beijing, China, 25–27 October 2017.
28. Elnail, K.E.; Huang, L.; Tan, L.; Wang, S.; Wu, X. Resonant Reactive Current Shield Design in WPT Systems for Charging EVs. In Proceedings of the 2018 IEEE PES Asia-Pacific Power and Energy Engineering Conference (APPEEC), Kota Kinabalu, Malaysia, 7–10 October 2018.

29. Park, J.; Ahn, S. A novel shielding coil for electromagnetic field(EMF) reduction of wireless power transfer in laptop computer. In Proceedings of the Wireless Power Transfer Conference, Jeju, Korea, 8–9 May 2014.
30. Tang, S.; Hui, S.; Chung, H.-H. Evaluation of the shielding effects on printed-circuit-board transformers using ferrite plates and copper sheets. *IEEE Trans. Power Electron.* **2002**, *17*, 1080–1088. [[CrossRef](#)]
31. Kunkel, G.M. *Shielding Theory and Practice*; In Proceedings of the 1992 Regional Symposium on Electromagnetic Compatibility, Tel-Aviv, Israel, 2–5 November 1992.
32. He, Y.; Ao, J.; Yang, J.; Tang, X. The Shielding-Effectiveness Based Magnetic Field Shielding Theory and Its Application in Mobile Payment Systems. In Proceedings of the 2014 IEEE 80th Vehicular Technology Conference (VTC2014-Fall), Vancouver, BC, Canada, 14–17 September 2014.
33. Kalwar, K.A.; Aamir, M.; Mekhilef, S. Inductively coupled power transfer (ICPT) for electric vehicle charging. *Renew. Sustain. Energy Rev.* **2015**, *47*, 462–475. [[CrossRef](#)]
34. Spaldin, N.A. *Magnetic Materials: Fundamentals and Applications*; Cambridge University Press: Cambridge, UK, 2011.
35. Jiang, Y.; Peterfy, C.G.; Zhao, J.J.; White, D.L.; Lynch, J.A.; Genant, H.K. Magnetic Resonance Imaging in Osteoarthritis. In *Osteoarthritis*; Springer: Berlin/Heidelberg, Germany, 1999.
36. Ramo S.; Whinner J.R.; Van Duzer T. *Fields and Waves in Communication Electronics*, 3rd ed.; John Wiley & Sons: Hoboken, NJ, USA 1994.
37. Tang, S.C.; Hui, S.Y.R.; Chung, H. Evaluation of the shielding effects on printed-circuit-board transformers using ferrite plates. In Proceedings of the 2001 IEEE 32ed Annual Power Electronics Specialists Conference, Vancouver, BC, Canada, 17–21 June 2001.
38. Kitano, Y.; Omori, H.; Morizane, T.; Kimura, N.; Nakaoka, M. A new shielding method for magnetic fields of a wireless EV charger with regard to human exposure by eddy current and magnetic path. In Proceedings of the 2014 International Power Electronics and Application Conference and Exposition, Shanghai, China, 5–8 November 2014.
39. Park, J.; Kim, D.; Hwang, K.; Park, H.H.; Kwak, S.I.; Kwon, J.H.; Ahn, S. A Resonant Reactive Shielding for Planar Wireless Power Transfer System in Smartphone Application. *IEEE Trans. Electromagn. Compat.* **2017**, *59*, 695–703. [[CrossRef](#)]
40. IEC Standard IEC 62110. *Electric and Magnetic Field Levels Generated by AC Power Systems: Measurement Procedures with Regard to Public Exposure*; IEC: Geneva, Switzerland, 2009.



© 2019 by the authors. Licensee MDPI, Basel, Switzerland. This article is an open access article distributed under the terms and conditions of the Creative Commons Attribution (CC BY) license (<http://creativecommons.org/licenses/by/4.0/>).